Optical Diagnostics For Non-Ideal Compressible Fluid Dynamics

Fabio Cozzi[1], Andrea Spinelli[1], Simone Gallarini[1], Alberto Guardone[2],

[1] *Dipartimento di Energia, Politecnico di Milano*
[2] *Dipartimento di Scienze e Tecnologie Aerospaziali, Politecnico di Milano*

Abstract

Optical based techniques are commonly employed in many technical and scientific fields, and those able to give qualitative and/or quantitative results about density and velocity fields are valuable tools to investigate compressible flows. In recent years a strong interest has emerged about non-ideal compressible flows also due to their relevance for variety of applications where such flows are encountered, including for example wind tunnels for aerodynamic testing and turbomachinery. Moreover, such flows theoretically show peculiar behaviour with respect to their ideal counterpart giving rise for example the possibility of rarefaction shocks to occur.

Actually very few examples of application of optical diagnostic techniques along with measured data are reported in the literature about non-ideal compressible flows. This work aim to present a brief summary of available optical techniques that are applied within the TROVA (Test Rig for Organic VApors) facility at the CREA laboratory of Politecnico di Milano. The TROVA test rig is designed to operate with siloxane, a family of silicon oil of particular interest for high temperature Organic Rankine Cycle (ORC) applications. MDM (Octamethyltrisiloxane-$C_8H_{24}O_2Si_3$) or either MM (Hexamethyldisiloxane-$C_6H_{18}OSi_2$) are currently used as a working fluid. To investigate such kind of flows innovative Schlieren and LDV techniques have been developed, tested and applied on the TROVA blow-down wind tunnel. The paper aims to provide a description of the measurement set-up used at CREA laboratory by considering also constraints and issues in their application and design. To support the conclusions, exemplary results achieved so far are reported.

1 Introduction

The interest towards non-ideal fluid dynamics has grown in recent years due to their relevance to industrial applications. Here, the term non-ideal is used to indicate the occurrence of peculiar flow behaviour because of departure from dilute, ideal-gas thermodynamics. It is interesting to observe that such kind of flows can theoretically show unusual phenomena; for example, in the so called non-classical regimes rarefaction shocks are physically admissible [1] [2]. More details about the theoretical analysis of so called non-classical regime can be found for example in [2, 1, 3, 4].

Optical techniques such as Schlieren and Laser Doppler Velocimetry (LDV) are a valuable tools to investigate compressible-fluid flows thanks to their ability to provide information about density gradients and flow velocities. Nevertheless, to the authors knowledge, example of their application to fluid flows featuring non-ideal behaviour close to liquid-vapour saturation and critical point, or within the supercritical region are still lacking.

The TROVA facility is a blow-down wind tunnel purposely designed to investigated non-ideal compressible-fluid flows by using, but not limited to, Schlieren and Laser Doppler Velocimetry (LDV) techniques. This paper offers a brief description on how those techniques have been successfully implemented, and it briefly analyses some constrains and issues for their application. Results achieved so far are reported.

2 The TROVA Wind Tunnel

The TROVA facility currently uses MDM (Octamethyltrisiloxane, $C_8H_{24}O_2Si_3$) and MM (Hexamethyldisiloxane, $C_6H_{18}OSi_2$) as working fluids. A detailed description of the TROVA test rig can be found in [5, 6, 7, 8, 9, 10, 11].

The TROVA wind tunnel has a 2D test section whose geometry can be easily changed. Straight and convergent-divergent channels are among available geometries. Convergent-divergent supersonic nozzles are designed according to a standard method of characteristics modified for dense gases [12]. A thick quartz window, installed on the channel side-wall, provides easy optical access for Laser Doppler Velocimetry and Schlieren technique, 2.1. It also allows for the Background Oriented Schlieren technique [13] to be implemented. A mirror-polished stainless steel plate is installed on the opposite side of the channel, and it hosts several equally spaced pressure taps for pressure measurements, see 2.1.

With reference to Figure (1), the wind tunnel operates as follows: the fluid stored in the closed high pressure vessel, is heated up to super-heated or supercritical conditions. By opening the Main Control Valve, the fluid is driven by the pressure gradient to flow through the systems down to the test section. Here, the channel geometry and the pressure difference between the inlet and outlet sections rule the flow expansion. The total pressure P_T and total temperature T_T are measured in the still chamber, element 6 in Figure (1), just ahead of the test section. The fluid discharged by the test section is collected into an ambient temperature and low pressure vessel (element 9 in Figure (1)) where it condenses. As the test proceeds the pressure difference between the high pressure and the low pressure vessels decreases until no pressure gradient exists in the system and the flow stops. As discussed in [5, 6] a steady flow within the nozzle can be assumed at any time during the test. The duration of a single run depends on several factors (pressure and temperature of the test, geometry of the test section etc.). In most of the investigated cases, test time is of the order of few minutes.

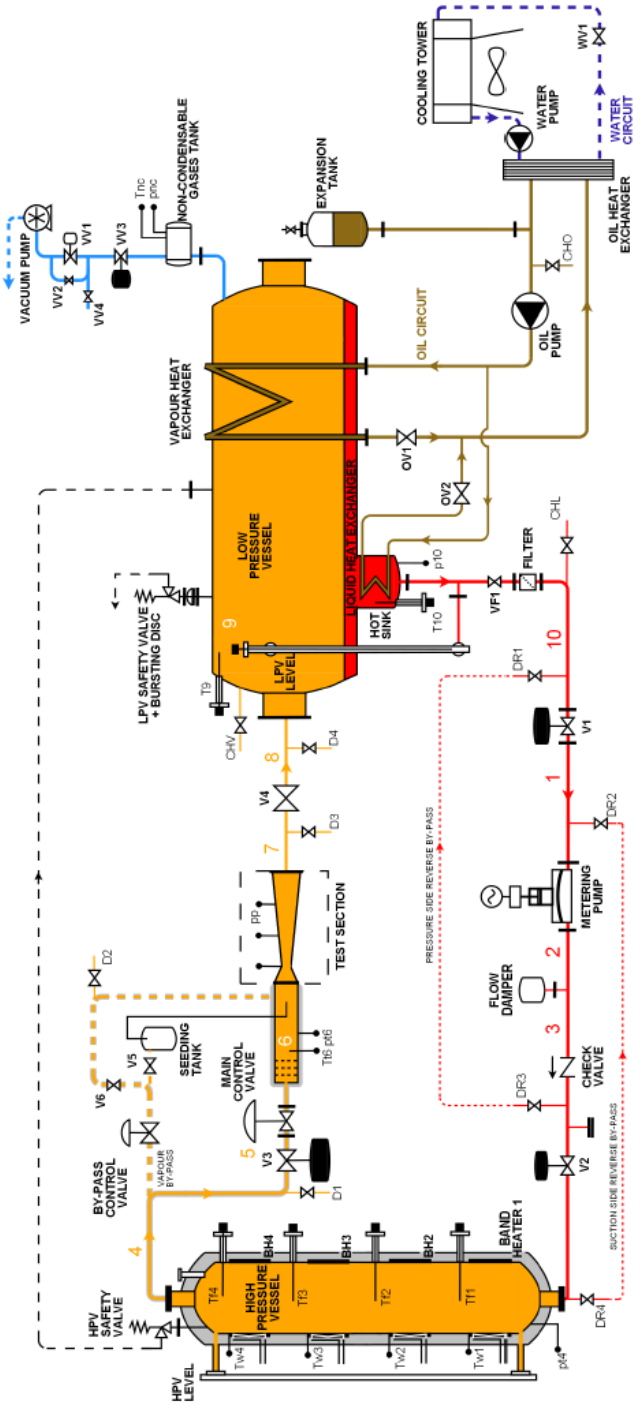

Figure 1: Sketch of the TROVA blow-down wind tunnel.

2.1 Schlieren technique

Since the optical access is restricted to one side of the channel, a double-pass Schlieren system is used, Figure (3). The diverging light beam from the light source is collimated by a bi-convex lens (L1, focal length $f_1 = 1000$ mm, diameter $d_1 = 150$ mm) and it enters at 90° with respect to the channel axis, Figure (3). Light rays deflected by density gradients in the fluid flow are reflected back by the mirror-polished rear plate 2.1. The reflected rays suffer a further deflection when crossing the fluid flow for the second time, then they focus at the knife edge by means of lens L1 (which now acts as the Schlieren head), after a 90° deflection operated by a cube beam splitter, Figure (3). The Schlieren image is formed onto the sensor of a high-speed CMOS camera by

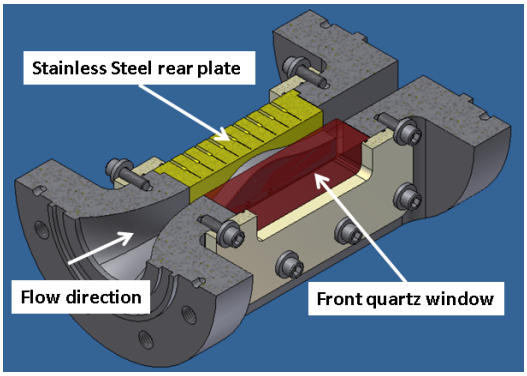

Figure 2: Cut view of the test section, stainless plate and the front quartz window for optical access are highlighted.

a second lens (L2, $f_2 = 75$ mm, diameter $d_2 = 52$ mm). The knife edge is oriented in the vertical direction so to visualize horizontal density gradients (i.e. those directed along the nozzle axis).

Either a blue led (OSRAM Ostar LEBQ9WN, dominant $\lambda = 460$ mm, emitting surface 0.9×0.9 mm^2) or a 100 W Hg arc-lamp have been used as a light sources. The LED light has proven to be a more versatile and stable light source than the Hg arc-lamp. Moreover, the LED can be pulsed and over-driven to improve light output. The mercury lamp also suffers from short terms and long terms light power fluctuations, it needs fans for cooling and it requires a warm up time of at least 1 h, so currently we use the LED as the preferred light source in Schlieren visualization.

To limit the cost of the mirror-polished rear plate, its quality is lower than that of common Schlieren mirrors. Nevertheless it is enough to ensure no significant disturbances in the Schlieren images. The polished surface gets dirty quite quickly, so its has to be cleaned every few tests if good contrast and sharpness in the Schlieren images are sought. Usually some drops of liquid working fluid or isopropyl alcohol are effective cleaning fluids, sometimes more strong solvents (such as acetone for example) are also employed, optical paper or a low lint optical tissue are used to wipe off the liquid. The same procedure is also used to clean the quartz windows.

The reflectivity of the stainless steel plate is somehow affected by the siloxane vapour, after few test the mirror surface assumes a slightly dark aspect, while the amount of light it reflects back to the Schlieren head decreases. This light reduction is compensated by increasing the light output of the lamp or either by increasing the exposure time when a continuous light source is used.

Schlieren images of siloxane flows can evidence measuring range issue as documented in [10, 14]. This problem arise in regions of strong density gradients (for example at the nozzle throat), where the light refraction is enough to deflect light onto some system aperture stop. Consequently, zone that should appear as a bright region can be totally or partially replaced by dark ones. An analysis of this issue was performed in [14] and more details can be found there. It is interesting to note the same issue is also described in [15] for Schlieren images of supersonic air flows.

2.1.1 Schlieren image analysis and results

Schlieren images easily provide qualitative data, nevertheless they can also provide quantitative data about lo-

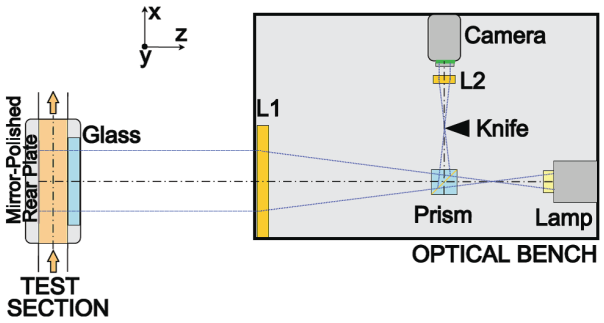

Figure 3: Sketch of the optical bench used for Schlieren visualizations, taken from [14].

cal Mach number, M, and instantaneous slope of shock waves. To this aim, an image analysis technique has been developed at CREA Laboratory to automatically detect straight flow structures such as oblique shock waves and simple waves in steady two-dimensional supersonic flows. The identification algorithm is based on the Hough transform, and it provides the slope, μ, of the straight flow structure. The Mach line slope with respect to the flow direction is directly linked to the Mach number, namely, $M = 1/sin\mu$. The detection of Mach lines allows a direct measurement of the local Mach number without involving any thermodynamic model in the calculation, if the direction of the velocity is known. A detailed description of the algorithm is reported in [16] and results can be found in [10, 11, 9, 16, 8].

As an example, a Schlieren image taken from [9] is shown in Figure (4). The Schlieren image refers to MDM vapors flowing in the diverging portion of a convergent-divergent supersonic nozzle. The Mach lines identified by the identification algorithm are superimposed on the same image as green segments. For this case total conditions are $P_{\mathrm{T}} = 9.2$ bar and $T_{\mathrm{T}} = 268$ °C, while the flow is in the non-ideal regime being the compressibility factor $Z_{\mathrm{T}} = 0.63$. The bottom part of Figure (4) shows the evolution of the Mach numbers along the nozzle axis, where green full symbols corresponds to Mach number computed from the Mach lines slope. CFD results (full green line), and Mach numbers (black empty symbols) computed from measured pressure and total conditions, i.e.P_{T} and T_{T}, are also reported on the same graph. The coherence of the three data sets is remarkable. Further details and comments can be found in [10, 11, 9, 16, 8].

2.2 Laser Doppler Velocimetry (LDV) technique

Laser Doppler Velocimetry (LDV) is a well established experimental technique used to investigate a wide range of complex flows and fluid-dynamic phenomena in transparent media, i.e. combustion flows, sprays, compressible flows, turbulent flows, coherent structures etc. A comprehensive review on principles, data analysis and practical implementation of the LDV technique can be found in [17]. To the authors knowledge, the present ones are the first LDV velocity measurements in a non-ideal supersonic flow of vapours. The aim of this section is to give an overview of the experimental set-up and of the methodologies used for LDV measurements.

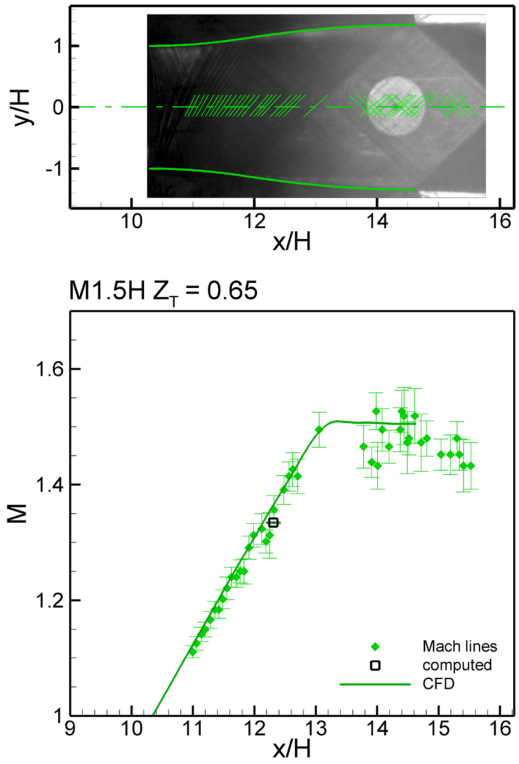

Figure 4: Schlieren image (top) and Mach numbers extracted from Mach lines (bottom), taken from [9].

2.2.1 Selection of the seeding material

The LDV technique requires the use of seeding particles dispersed in the flow, a proper choice of the seeding particles is of paramount importance to get accurate fluid velocity measurements [17].

First, the seeding material has to be chemically compatible with the fluid under investigation. Chemical modification induced by the seeding particles can alter the thermo-fluid dynamic behaviour of the fluid, jeopardizing the possibility to correctly understand the experimental outcome. Moreover even for chemically compatible seeding materials, a high melting temperature solid seeding has the advantages to be much less prone to evaporate than a liquid one, so it could be a preferred choice at flow temperatures above the ambient one. For example, in our tests, and depending on the operating conditions, the siloxane vapour expands in the TROVA nozzle starting from total pressure and total temperature of the order of about 9 bar and 250 °C, respectively.

The basic requirement of any tracer is to faithfully follow the flow velocity. This requires the response time of the particle, τ_p, to be much smaller than the characteristic time of the flow τ_f, i.e. the particle Stokes number needs to be $\mathrm{St} = \tau_p/\tau_f \ll 1$ [17, 18]. For ideal seeding particles the particle to fluid density ratio, $\zeta = \rho_p/\rho_f$, is equal to 1, thus they instantaneously and perfectly adjusts their velocity to that of the flow and no velocity slip exists between the particles and the flow [17, 18]. Unfortunately, such ideal situation can hardly be realized, thus a trade-off is required between small particle diameters, for fast response to velocity fluctuations, and large particle diameter, for a high signal-to-noise ratio (SNR) of the scattered light signal. The latter also increases with the ratio of the refractive indexes of the seeding particle n_p to that of the fluid, n_f thus high refractive index materials should be preferred as seeding.

Table 1: Physical properties of seeding materials

Material	Refractive index	Density kg/m^3	Melting Point °C
TiO_2	$2.6 - 2.9$	$3900 - 4200$	1840
Al_2O_3	1.79	3960	2015
SiO_2	1.45	2200	1710
SiC	2.6	3200	2700

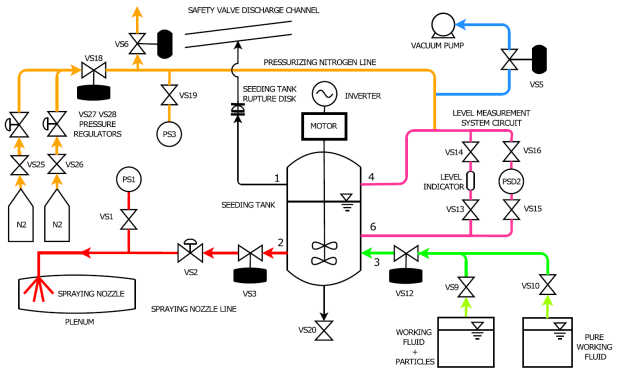

Figure 5: Sketch of the seeding system.

Finally, the flow temperatures in excess of 200 °C restricted our choices to the solid materials shown in Table (1), which are commonly used as seeding in LDV and PIV measurements [19, 17]. By taking all the constrains into account, TiO_2 resulted to be the most suitable material. The other materials have a much lower refractive index (SiO_2 and Al_2O_3), or being very hard can scratch the quartz windows more easily (SiC). Nanosized TiO_2 powder, with clusters diameter in the range $150 - 250$ nm, satisfies the constraint on Stokes number ($St \ll 1$). The analysis on the dynamic response of nanosized TiO_2 particles is reported in [20, 21].

2.2.2 Seeding system

To inject the seeding we resort to the use of a liquid suspension of TiO_2 powder, where the liquid is the same fluid used in the wind tunnel. The TiO_2 powder is dried in a oven at $T > 100$ °C for at least one hour before being dispersed in the liquid, to avoid moisture contamination. The liquid suspension is put in a tank, 2.2.2, and pressurized with nitrogen at about 9 bar above the maximum stagnation pressure of the test. As shown in 2.2.2, two vertical axis blade impellers actuated by an electrical motor are located inside the tank. The impellers rotation creates an intense flow re-circulation preventing the seeding to settle down and keeping the liquid suspension homogeneous. The impeller stirring device performs much better than the mixing nozzle used in our previous design [20]. When the test starts, the valve VS3 in 2.2.2 is opened and the liquid suspension is forced by pressure to the atomizing nozzle located in the section ahead of the nozzle inlet, see Figure (1) and 2.2.2. A full cone nozzle atomizer is used. Since the surrounding fluid is in super-heated vapour (or supercritical) conditions, the spray evaporates leaving the solid particles free to follow the flow. The sketch of the seeding system layout is shown 2.2.2.

The mass of powder required for the liquid suspension is estimated by considering the need to have no more than one particles in the LDV measurement volume. By imposing a probability of 0.5% that two or more particles are in the measurement volume at the same time,

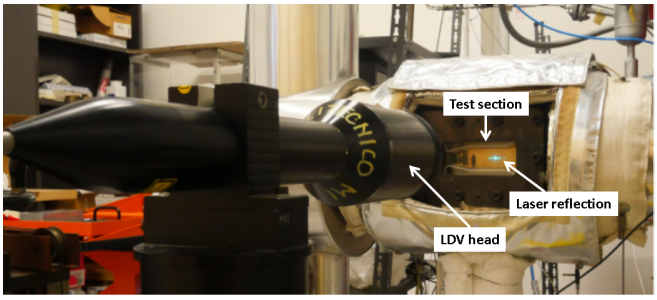

Figure 6: LDV head and tests section.

the maximum particle concentration, n_p, in the measurement volume, V_m, is computed as [17]

$$\mathrm{n_p} = \frac{0.1}{\mathrm{V_m}}; \qquad (1)$$

Using Eq. (1), the local particle flow rate is $N_p = 0.1\dot{V}_f/V_m$, where $\dot{V}_f$ is the volumetric flow rate at the measurement section. Eventually, the required mass of seeding m_p is computed as $m_p = \frac{4}{3}\pi d_p^3 \rho_p \frac{0.1}{V_m}\dot{V}_f \Delta t$ where Δt is the total measurement time. Actually not all the seeding particles reach the measurements location, thus the optimum values of m_p needs to be found from empirical observation of data rate and signal quality. The amount of liquid needed for the suspension depends on the atomizing nozzle and on pressure drop imposed across it, thus it has to be adjusted according to the set-up and the operating conditions. In any case, it is recommended to keep its quantity as small as possible so to minimize any influence the liquid spray can have on flow conditions.

2.2.3 LDV system

To avoid the burden of using a separate receiving optics, which would pose significant alignment issues, the LDV system operates in the back-scatter mode. The LDV uses two Diode Pumped Solid State (DPSS) lasers, each having a maximum output power of 1 W. The lasers wavelength are $\lambda = 513.9$ nm and $\lambda = 489.5$ nm. Both laser beams have a diameter of about $d_{\mathrm{lb}} = 1$ mm. The latters are input to a Dantec Fiberflow transmission system, where a Bragg cell acts as a beam splitter and as a 40 MHz frequency shifter. Fiber-optic transmits the two frequency-shifted couples of laser beams from the Fiberflow to the LDV head. The light scattered by the particle is collectd by the LDV head and sent to the photo multiplier via a fiber-optic.

The LDV head, Figure (6), is composed by a beam expander (expander ratio of about 1.87) and a frontal lens of focal length $f = 310$ mm and about 80 mm diameter. Each couple of laser beams intersect with a semi-angle of about $\theta/2 = 6.5°$, resulting in a measurement volume of about 0.006 mm^3, Table (2). The LDV head is mounted on a XY manual translation stage to allow the accurate positioning of the measurement volume on the channel axis.

Doppler signals are analysed by a Burst Spectrum Analyzer (Dantec Dynamics BSA F800) controlled via a USB connection by a PC. Instantaneous velocities, Doppler burst signals, data rate and burst validation percentage are some of the information provided by the BSA. This allows to promptly identify measurements issues during the test, and if needed to stop the test. A single TTL signal is used to trigger both the BSA system

Table 2: Computed optical specifications of the LDV probe volume (in air)

Optical Parameters			units
Focal length,f	310	310	mm
Wavelengths, λ	513.9	489.5	nm
Beam intersection angle, θ	0.23	0.23	rad
Measuring volume diameter	0.109	0.104	mm
Measuring volume length	≈ 1	≈ 1	mm
Measuring volume, V_m	0.006	0.005	mm^3
Fringe distance	2.24	2.13	μm
Fringe number	48	48	

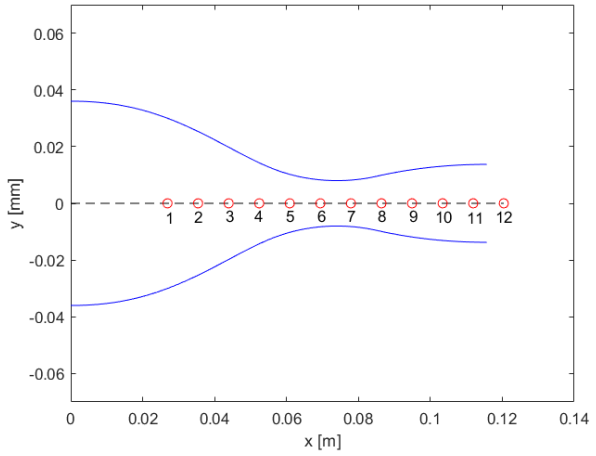

Figure 7: Sketch of the 2D convergent-divergent nozzle, red circles show the locations of pressure taps.

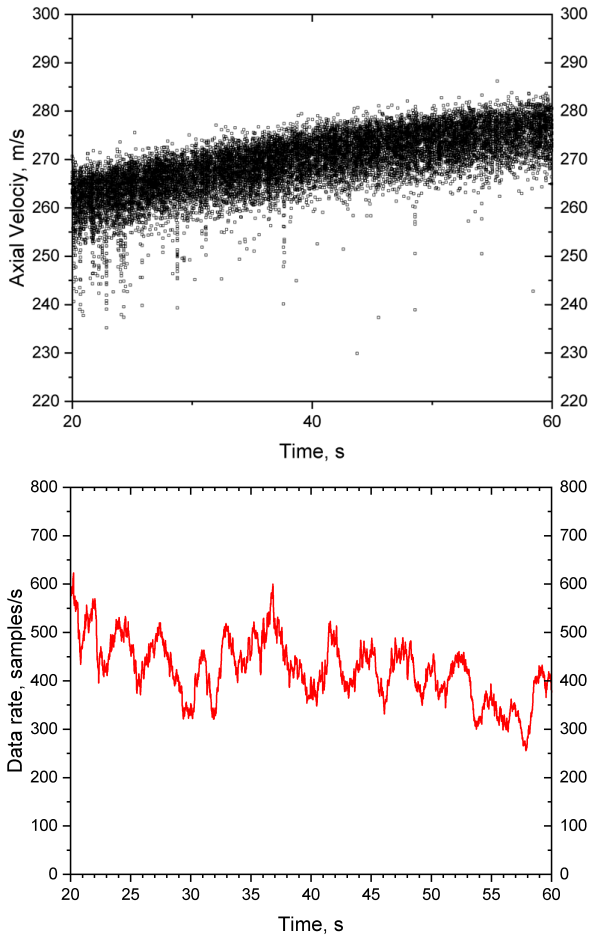

Figure 8: Top: measured axial velocity. Bottom: LDV data rate, moving average $\sim$ 1 s window.

and the pressures and temperatures acquisition system, to allow all measurements to be easily re-aligned in time and correctly compared.

When dealing with high speed flow, the optical configuration of the LDV head has to ensure a maximum Doppler frequencies below the maximum value accepted by the Burst Spectrum Analyzer, $f_{D,\max}$. The constraint is satisfied if the angle between the two laser beams is below the value $\theta_{\max}$ given by Eq. (2), where V is the maximum expected flow velocity.

$$\frac{1}{2}\theta_{\max} = \arcsin\left(\frac{\lambda}{2V} f_{D,\max}\right) \qquad (2)$$

In the present case, BSA specifications gives $f_{D,\max} =$ 200 MHz (Dantec Dynamics BSA F800), while $V \approx 300$ m/s and $\lambda = 513.9$ nm. Thus, from Eq. (2) we get $\theta_{\max}/2 \approx 9°$, corresponding to a minimum usable focal length $f = 200$ mm. We chose a lens having $f = 310$ mm because besides satisfying the above constraint, it also allows a suitable space between the hot test section and the LDV head.

The probe volume generated by the 310 mm is about 1 mm in length, the short length size greatly reduce the amount of laser light picked up by the LDV head due to beam reflection at the metallic rear plate, Figure (6). More details about the optical specifications of the probe volume are shown in Table (2).

2.2.4 LDV measurements

Velocity measurements have been performed on different channel geometries (2D Convergent-Divergent nozzle and 2D subsonic straight channels) using MM as a working fluid; here just one example of velocity measurements taken in the 2D supersonic converging diverging nozzle is reported, Figure (7). The LDV measurement volume was located in the symmetry plane of the 2D channels, and in front of the pressure tap 11 shown in Figure (7), i.e. at axial location close to the nozzle exit.

Using a laser power of about 150 mW, the data rate (mean over 1 s) varied between about 5 kHz and 0.2 kHz decreasing during the tests, see Figure (8)(b), while data validation was always above 95%. At the beginning of the test we measured $P_T \approx 8.4$ bar and $T_T \approx 207$ °C. Being a blow-down wind tunnel, the total pressure decreases significantly during the test. On the other side, due to the high molecular complexity of MM, the total temperature changes only slightly. The total compressibility factor Z_T increases from about 0.75 to a value close to 1 [21]. Thus, the thermodynamic conditions of the flow moves away from the non-ideal region and approaches the ideal gas region as the test proceeds. As an example only velocities measured during the time interval between 20 s to 60 s from the start of the test are shown in Figure (8)(a). The axial velocity clearly increases from about 260 m/s to about 275 m/s, Figure (8). This behaviour can be attributed to the increase of Z_T and it is an indication of the non-ideality of the flow. Moreover, LDV measurements were compared to velocity estimated using the static pressure at pressure tap 11, not reported here, resulting in good agreement between each other [21]. This result further support the validity of the design of the LDV system.

3 Conclusions

Optical techniques such as Schlieren and Laser Doppler Velocimetry (LDV) are valuable tools to investigate compressible flows thanks to their ability to provide information about density gradients, Mach number and flow velocity. Nevertheless, to the authors knowledge, example of their application to fluid flows featuring non-ideal behaviour close to saturation and critical point, or within the supercritical region, are currently not available.

The present paper reported for the first time on the use of Schlieren and Laser Doppler Velocimetry (LDV) techniques to measure non-ideal compressible-fluid flows. All measurements where carried out within the blow-down TROVA facility at Politecnico di Milano. Peculiar aspects of the design and implementation are described. Measurement are reported including Mach number measurements along the nozzle axis and velocity measurements in highly non-ideal conditions.

Acknowledgment

This research is supported by ERC Consolidator Grant N. 617603, Project NSHOCK, funded under the FP7-IDEAS-ERC scheme.

References

[1] M. Cramer, "Nonclassical dynamics of classical gases," in *Nonlinear waves in real fluids*, pp. 91–145, Springer, 1991.

[2] P. A. Thompson, "A fundamental derivative in gasdynamics," *The Physics of Fluids*, vol. 14, no. 9, pp. 1843–1849, 1971.

[3] A. Kluwick, "Rarefaction shocks," in *Handbook of shock waves*, pp. 339–411, Elsevier, 2001.

[4] A. Guardone, P. Colonna, E. Casati, and E. Rinaldi, "Non-classical gas dynamics of vapour mixtures," *Journal of fluid mechanics*, vol. 741, pp. 681–701, 2014.

[5] A. Spinelli, V. Dossena, P. Gaetani, C. Osnaghi, and D. Colombo, "Design of a test rig for organic vapours," in *ASME Turbo Expo 2010: Power for Land, Sea, and Air*, pp. 109–120, American Society of Mechanical Engineers Digital Collection, 2010.

[6] A. Spinelli, M. Pini, V. Dossena, P. Gaetani, and F. Casella, "Design, simulation, and construction of a test rig for organic vapors," *Journal of engineering for gas turbines and power*, vol. 135, no. 4, 2013.

[7] A. Spinelli, F. Cozzi, V. Dossena, P. Gaetani, M. Zocca, and A. Guardone, "Experimental investigation of a non-ideal expansion flow of siloxane vapor mdm," in *ASME Turbo Expo 2016: Turbomachinery Technical Conference and Exposition*, American Society of Mechanical Engineers Digital Collection, 2016.

[8] A. Spinelli, G. Cammi, M. Zocca, S. Gallarini, F. Cozzi, P. Gaetani, V. Dossena, and A. Guardone, "Experimental observation of non-ideal expanding flows of siloxane mdm vapor for orc applications," *Energy Procedia*, vol. 129, pp. 1125–1132, 2017.

[9] A. Spinelli, G. Cammi, S. Gallarini, M. Zocca, F. Cozzi, P. Gaetani, V. Dossena, and A. Guardone, "Experimental evidence of non-ideal compressible effects in expanding flow of a high molecular complexity vapor," *Experiments in Fluids*, vol. 59, no. 8, p. 126, 2018.

[10] A. Spinelli, G. Cammi, C. C. Conti, S. Gallarini, M. Zocca, F. Cozzi, P. Gaetani, V. Dossena, and A. Guardone, "Experimental observation and thermodynamic modeling of non-ideal expanding flows of siloxane mdm vapor for orc applications," *Energy*, vol. 168, pp. 285–294, 2019.

[11] M. Zocca, A. Guardone, G. Cammi, F. Cozzi, and A. Spinelli, "Experimental observation of oblique shock waves in steady non-ideal flows," *Experiments in Fluids*, vol. 60, no. 6, p. 101, 2019.

[12] A. Guardone, A. Spinelli, and V. Dossena, "Influence of molecular complexity on nozzle design for an organic vapor wind tunnel," *Journal of engineering for gas turbines and power*, vol. 135, no. 4, 2013.

[13] F. Cozzi, E. Göttlich, L. Angelucci, V. Dossena, and A. Guardone, "Development of a background-oriented schlieren technique with telecentric lenses for supersonic flow," in *Journal of Physics: Conference Series*, vol. 778, p. 012006, IOP Publishing, 2017.

[14] C. C. Conti, A. Spinelli, G. Cammi, M. Zocca, F. Cozzi, and A. Guardone, "Schlieren visualizations of non-ideal compressible fluid flows," in *13th International Conference on Heat Transfer, Fluid Mechanics and Thermodynamics (HEFAT 2017)*, pp. 513–518, EDAS, 2017.

[15] W. Mair, "The sensitivity and range required in a toepler schlieren apparatus for photography of high-speed air flow," *The Aeronautical Quarterly*, vol. 4, no. 1, pp. 19–50, 1954.

[16] G. Cammi, *Measurements techniques for non-ideal compressible fluid flows: applications to organic fluids*. PhD thesis, Politecnico di Milano, 2019.

[17] H.-E. Albrecht, N. Damaschke, M. Borys, and C. Tropea, *Laser Doppler and phase Doppler measurement techniques*. Springer Science & Business Media, 2013.

[18] R. Mei, "Velocity fidelity of flow tracer particles," *Experiments in fluids*, vol. 22, no. 1, pp. 1–13, 1996.

[19] A. Melling, "Tracer particles and seeding for particle image velocimetry," *Measurement science and technology*, vol. 8, no. 12, p. 1406, 1997.

[20] S. Gallarini, A. Spinelli, F. Cozzi, and A. Guardone, "Design and commissioning of a laser doppler velocimetry seeding system for non-ideal fluid flows," 12th International Conference on Heat Transfer, Fluid Mechanics and Thermodynamics, HEFAT, 2016.

[21] S. Gallarini, *High Temperature non-ideal compressible-fluid flows of siloxane*. PhD thesis, Politecnico di Milano, 2020.